Journal of Power Sources 193 (2009) 431–440

Contents lists available at ScienceDirect

Journal of Power Sources

journal homepage: www.elsevier.com/locate/jpowsour

Cathode reaction mechanism of porous-structured $Sm_{0.5}Sr_{0.5}CoO_{3-\delta}$ and $Sm_{0.5}Sr_{0.5}CoO_{3-\delta}/Sm_{0.2}Ce_{0.8}O_{1.9}$ for solid oxide fuel cells

Seung-Wook Baek[a], Joongmyeon Bae[a,*], Young-Sung Yoo[b]

[a] Department of Mechanical Engineering, Korea Advanced Institute of Science and Technology (KAIST), 373-1 Guseong-Dong, Yuseong-Gu, Daejeon 305-701, Republic of Korea
[b] Korea Electric Power Research Institute (KEPRI), Daejeon 305-380, Republic of Korea

ARTICLE INFO

Article history:
Received 18 January 2009
Received in revised form 15 March 2009
Accepted 16 March 2009
Available online 14 April 2009

Keywords:
Cathode reaction
Samarium oxide
Solid oxide fuel cell

ABSTRACT

The cathode reaction mechanism of porous $Sm_{0.5}Sr_{0.5}CoO_{3-\delta}$, a mixed ionic and electronic conductor (MIEC), is studied through a comparison with the composite cathode $Sm_{0.5}Sr_{0.5}CoO_{3-\delta}/Sm_{0.2}Ce_{0.8}O_{1.9}$. First, the cathodic behaviour of porous $Sm_{0.5}Sr_{0.5}CoO_{3-\delta}$ and $Sm_{0.5}Sr_{0.5}CoO_{3-\delta}/Sm_{0.2}Ce_{0.8}O_{1.9}$ are observed for micro-structure and impedance spectra according to $Sm_{0.2}Ce_{0.8}O_{1.9}$ addition, thermal cycling and long-term properties. The cathode reaction mechanism is discussed in terms of frequency response, activation energy, reaction order and electrode resistance for different oxygen partial pressures $p(O_2)$ at various temperatures. Three elementary steps are considered to be involved in the cathodic reaction: (i) oxygen ion transfer at the cathode–electrolyte interface; (ii) oxygen ion conduction in the bulk cathode; (iii) gas phase diffusion of oxygen. A reaction model based on the empirical equivalent circuit is introduced and analyzed using the impedance spectra. The electrode resistance at high frequency ($R_{c,HF}$) in the impedance spectra represents reaction steps (i), due to its fast reaction rate. The electrode resistance at high frequency is independent of $p(O_2)$ at a constant temperature because the semicircle of $R_{c,HF}$ in the complex plane of the impedance spectra is held constant for different values of $p(O_2)$. Reaction steps (ii) and (iii) are the dominant processes for a MIEC cathode, according to the analysis results. The proposed cathode reaction model and results for a solid oxide fuel cell (SOFC) well describe a MIEC cathode with high ionic conductivity, and assist the understanding of the MIEC cathode reaction mechanism.

1. Introduction

The design of cathode materials is very important due to their large over potentials, especially in a solid oxide fuel cell (SOFC). One type of conventional cathode, known as LSM (lanthanum strontium manganite), has been widely used [1–5], but exhibits relatively low electrocatalytic activity. Mixed ionic and electronic conductors (MIECs) have recently gained attention due to their good electrochemical properties, despite their low stability [6–22]. An understanding of the differences in the cathode reaction mechanisms between conventional cathodes and MIECs is necessary in the design of a high-performance fuel cell.

Several important studies concerning the cathode reaction mechanism have been reported. Deseure et al. [5] reported an oxygen reduction mechanism effect based on a one-dimensional homogeneous model for the porous cathode. A LSM-YSZ composite cathode was modelled, and the rate-determining steps (RDSs) were discussed according to the frequency range and the effect of the micro-structure. Adler et al. [16] examined the contribution of gas phase diffusion and the RDS for a p-type material using a continuum model. Horita et al. [13] studied on the oxide ion conduction and surface oxygen exchange of a LSC (lanthanum strontium cobaltite) cathode with respect to the effect of cathodic over potential on the reaction rate. Hunsom et al. [14] investigated the influence of the firing temperature on a LSC/SDC cathode and analyzed the RDS according to the frequency range. Critical discussion of the reaction order and the electrochemical reaction itself for LSC systems was presented by Takeda et al. [3]. Fukunaga et al. [11] studied the oxygen reduction mechanism for both a dense and a porous SSC55 cathode. The authors proposed a different model from that of Adler et al. for a MIEC cathode based on an empirical equivalent circuit model. Esquirol et al. [9] discussed oxygen transport in a composite MIEC cathode with respect to oxygen bulk conduction and surface diffusion.

In the present study, the oxygen reduction reaction on a porous-structured cathode manufactured from $Sm_{0.5}Sr_{0.5}CoO_{3-\delta}$ and on a related composite cathode, $Sm_{0.5}Sr_{0.5}CoO_{3-\delta}/Sm_{0.2}Ce_{0.8}O_{1.9}$, is investigated in terms of micro-structure, impedance spectra, and the oxygen partial pressure ($p(O_2)$) dependence at various temperatures. Three elementary RDSs are mainly involved in the cathodic reaction: (i) oxygen ion transfer at the interface of the cathode and

* Corresponding author. Tel.: +82 42 869 3045; fax: +82 42 869 8207.
E-mail addresses: baeksw77@kaist.ac.kr (S.-W. Baek), jmbae@kaist.ac.kr (J. Bae), yungsung@kepri.re.kr (Y.-S. Yoo).

0378-7753/$ – see front matter © 2009 Elsevier B.V. All rights reserved.
doi:10.1016/j.jpowsour.2009.03.071

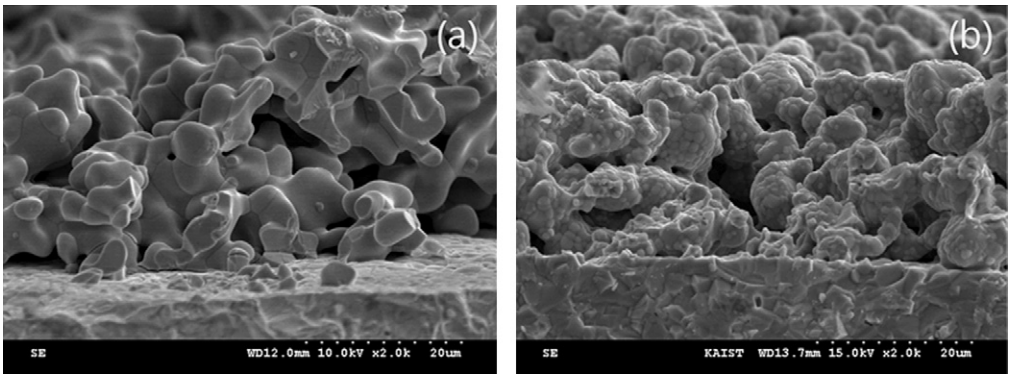

Fig. 1. Changes in cathode microstructure to the addition of $Sm_{0.2}Ce_{0.8}O_{1.9}$. (a) $Sm_{0.5}Sr_{0.5}CoO_{3-\delta}$ and (b) $Sm_{0.5}Sr_{0.5}CoO_{3-\delta}/Sm_{0.2}Ce_{0.8}O_{1.9}$.

the electrolyte, (ii) oxygen ion conduction in the bulk cathode and (iii) gas phase diffusion of oxygen. The relationship between the cathode reaction process and the reaction order is evaluated to determine the RDS.

2. Experimental methods

2.1. Preparation

$Sm_{0.5}Sr_{0.5}CoO_{3-\delta}$ was synthesized using the glycine nitrate process (GNP). $Sm(NO_3)_3 6H_2O$, $Sr(NO_3)_2$, $Co(NO_3)_2 6H_2O$ and glycine were prepared in weighed mole ratios. The prepared nitrate and glycine were dissolved in de-ionized water, and the solution was heated to 300 °C. The cathode powder was calcined for 1 h at 1250 °C to remove residual carbon and to crystallize the structure. $Sm_{0.2}Ce_{0.8}O_{1.9}$ was prepared using a commercial powder (Praxair) as an electrolyte material. A $Sm_{0.5}Sr_{0.5}CoO_{3-\delta}/Sm_{0.2}Ce_{0.8}O_{1.9}$ composite cathode was prepared via the ethanol-based ball mill method. $Sm_{0.5}Sr_{0.5}CoO_{3-\delta}$ and $Sm_{0.2}Ce_{0.8}O_{1.9}$ were mixed at a weight ratio of 6:4. $Sm_{0.5}Sr_{0.5}CoO_{3-\delta}$ and $Sm_{0.5}Sr_{0.5}CoO_{3-\delta}/Sm_{0.2}Ce_{0.8}O_{1.9}$ were screen-printed on to $Sm_{0.2}Ce_{0.8}O_{1.9}$ electrolyte pellets with a thickness of 1 mm and a diameter of 23 mm. The thickness of the cathode layer, measured by means of a scanning electron microscope (SEM), was 20–50 μm. A $Sm_{0.2}Ce_{0.8}O_{1.9}$ electrolyte pellet was created through a process of uni-axial pressing under a weight of 50 $kg_f\,cm^{-2}$. The prepared half-cells were then sintered for 1 h at 1200 °C.

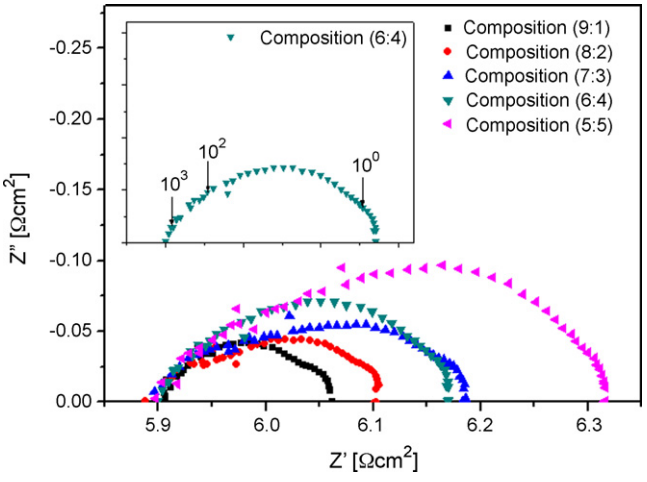

Fig. 2. Impedance spectra variation according to amount of $Sm_{0.2}Ce_{0.8}O_{1.9}$ addition. *Composition (6:4): $Sm_{0.5}Sr_{0.5}CoO_{3-\delta}/Sm_{0.2}Ce_{0.8}O_{1.9}$ (6:4).

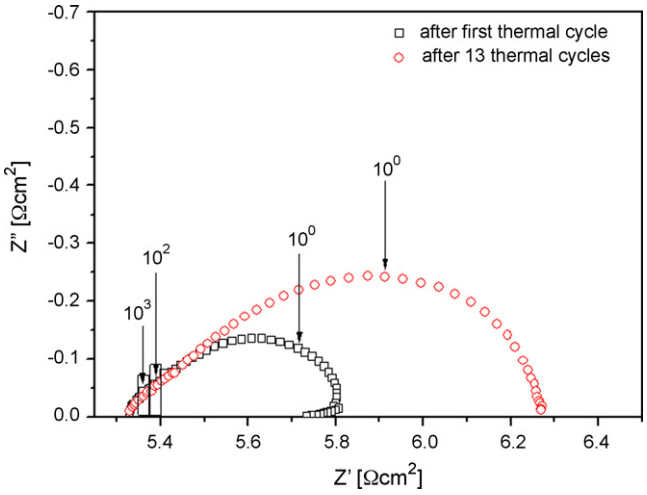

Fig. 3. Impedance spectra for thermal cycle test of $Sm_{0.5}Sr_{0.5}CoO_{3-\delta}$.

2.2. Measurement

An four-probe method was used to measure the electrochemical a.c. impedance. Measurements were conducted in the temperature range of 450–900 °C and in pre-mixed O_2–N_2 gas. The oxygen partial pressure $p(O_2)$ ranged from 0.0002 to 1 atm. The measurement was performed with a Solartron 1287/Solartron 1260 (electrochemical interface/impedance, gain-phase analyzer) device and the Z

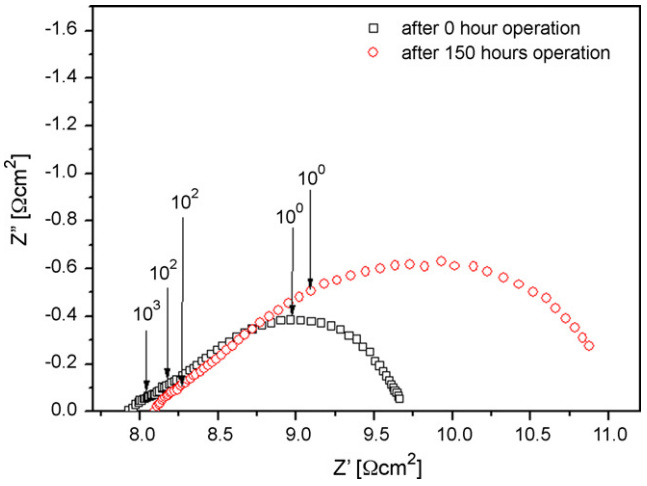

Fig. 4. Impedance spectra for long-term test of $Sm_{0.5}Sr_{0.5}CoO_{3-\delta}$.

View commercial program. The frequency range was 5×10^6 to 1×10^{-2} Hz and the applied voltage amplitude was 20 mV.

3. Results and discussion

3.1. Micro-structure and impedance spectra variation

In previous research, the addition of $Sm_{0.2}Ce_{0.8}O_{1.9}$ to $Sm_{0.5}Sr_{0.5}CoO_{3-\delta}$ was found to have a large effect on the coefficient of thermal expansion, thermal cycling stability and enhancement of electrochemical performance [23]. The significant difference of the microstructure of $Sm_{0.5}Sr_{0.5}CoO_{3-\delta}$ and $Sm_{0.5}Sr_{0.5}CoO_{3-\delta}/Sm_{0.2}Ce_{0.8}O_{1.9}$ is demonstrated in Fig. 1. It is certain that the addition of $Sm_{0.2}Ce_{0.8}O_{1.9}$ plays an important role in the enhanced of sinterability of particles and adhesion to the electrolyte. The influence of $Sm_{0.2}Ce_{0.8}O_{1.9}$ addition on the microstructure can be verified from impedance spectra. An investigation by impedance spectroscopy gives valuable insight into the reaction mechanism [4–6,12–15,21,22,24,25]. As shown in Fig. 2, the addition of $Sm_{0.2}Ce_{0.8}O_{1.9}$ clearly affects the impedance in the 100–1 Hz frequency range. The impedance spectra do not significantly change for frequencies above 100 Hz and below 1 Hz. It is known that the addition of $Sm_{0.2}Ce_{0.8}O_{1.9}$ enhances the ionic conduction of the bulk media in the cathode. Thus, the reaction processes for the frequency ranges of 100–1 Hz and below 1 Hz are related to ionic

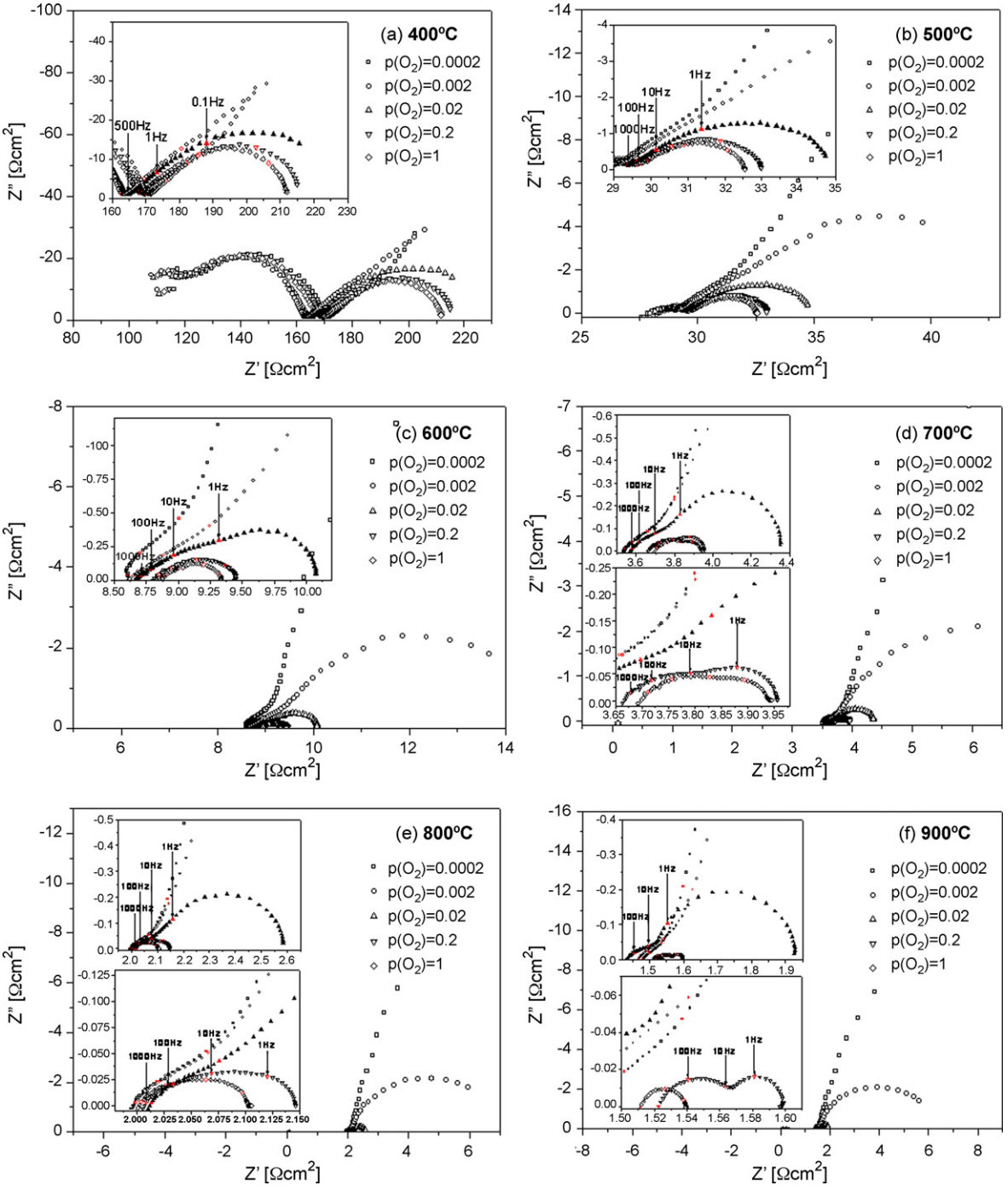

Fig. 5. Impedance spectra of single phase $Sm_{0.5}Sr_{0.5}CoO_{3-\delta}$ cathode with variation in oxygen partial pressure $p(O_2)$ and operating temperature.

conduction and gas phase diffusion, respectively. Figs. 3 and 4 show the impedance spectra variation for thermal cycling and long-term performance of $Sm_{0.5}Sr_{0.5}CoO_{3-\delta}$, respectively. The effects of cracks in the cathode particles and delamination between the electrolyte and cathode can be verified from the thermal cycling test. In the present research, thermal cycle degradation may also be affected by degradation due to long-term operation. The long-term performance test shows that the resistance in the frequency range greater than 1 Hz does not change but that the resistance in the frequency range less than 1 Hz increases significantly. The effect of the long-term degradation is clearly represented in the frequency range under 1 Hz. Thus, performance degradation via the pure thermal cycling effect of $Sm_{0.5}Sr_{0.5}CoO_{3-\delta}$ is prevalent in the approximate frequency range of 100–1 Hz, as shown in Fig. 3. As a result, the addition of $Sm_{0.2}Ce_{0.8}O_{1.9}$ influences the connection of cathode particles and their adhesion to electrolyte, and plays an important role in the cathode reaction of MIEC. These effects are clearly shown in the medium frequency range of 100–1 Hz.

3.2. Impedance spectra for $p(O_2)$ and temperature

The variation in $Sm_{0.5}Sr_{0.5}CoO_{3-\delta}$ impedance spectra with respect to $p(O_2)$ and temperature is presented in Fig. 5. Fig. 5(a) and (b) shows the grain boundary resistance of the electrolyte that occurs at frequencies greater than 10^3 Hz. This grain boundary resistance disappears as the temperature increased. Three

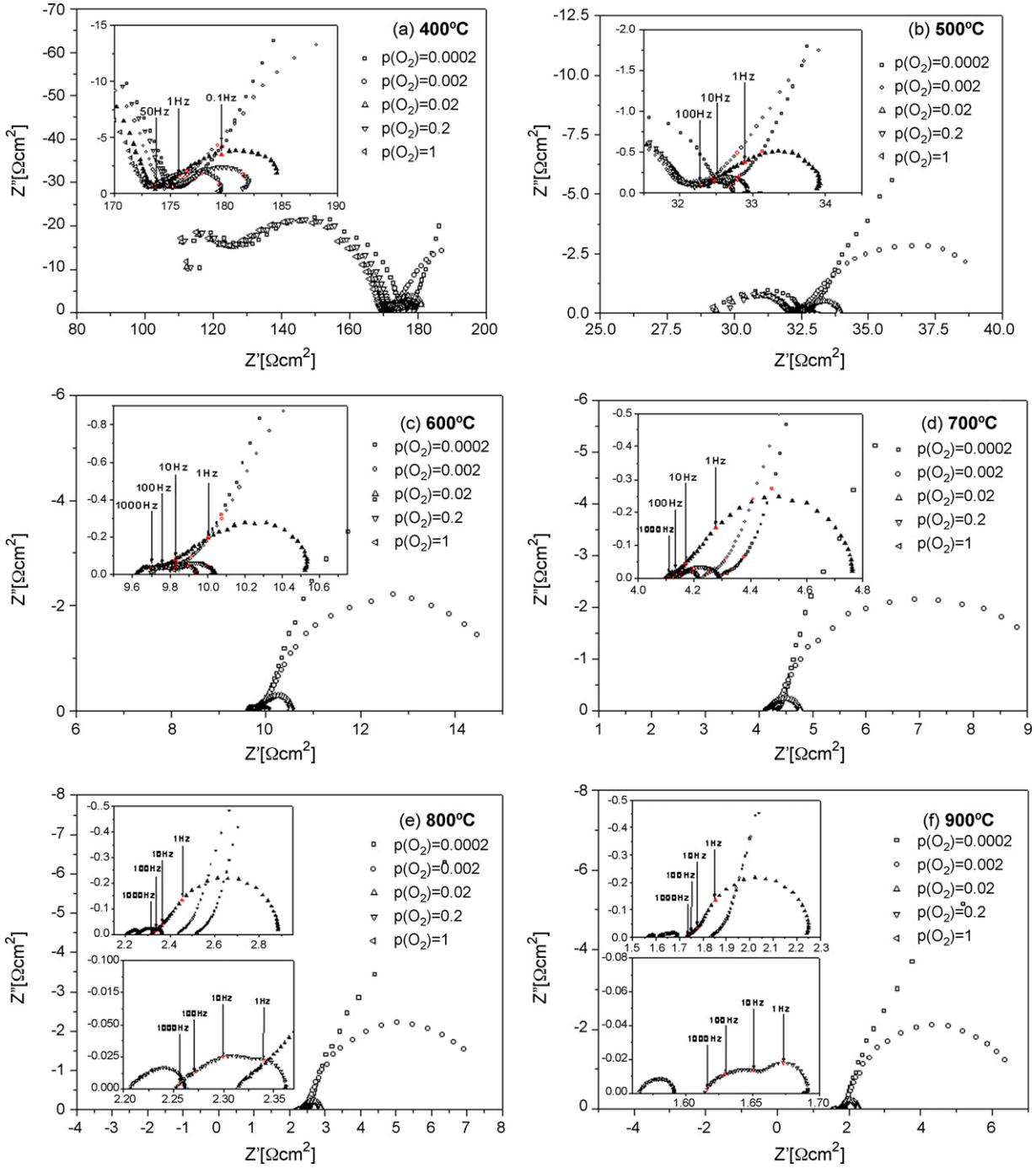

Fig. 6. Impedance spectra of $Sm_{0.5}Sr_{0.5}CoO_{3-\delta}/Sm_{0.2}Ce_{0.8}O_{1.9}$ (6:4) composite cathode with variation in oxygen partial pressure $p(O_2)$ and operating temperature.

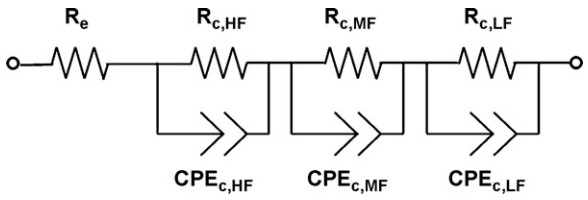

Fig. 7. Equivalent circuit model with constant phase elements (CPEs). $^*R_e$: electrolyte resistance; $R_{c,HF}$: electrode resistance at high frequency; $R_{c,MF}$: electrode resistance at medium frequency; $R_{c,LF}$: electrode resistance at low frequency.

semicircles are evident from the impedance results. The resistance in the high-frequency region (10^3–10^2 Hz) is independent of $p(O_2)$ in the range of 0.0002–1 atm. The resistance in the low-frequency region (below 1 Hz) clearly changes as the value of $p(O_2)$ increases. By contrast, a change in the resistance related to the medium-frequency region (100–1 Hz) is not apparent. The distribution and boundary of the characteristic frequency are apparent for the $p(O_2)$ value and temperature ranges. The range of the low-frequency appeares to be less than 1 Hz at 700 °C at a pressure of 0.02 atm, but, it is considered to be less than 10 Hz at 900 °C at 0.2 atm. This difference is acceptable when analyzing the impedance spectra. The impedance spectra provide key information for the establishment of an equivalent model and in the analysis of the oxygen reduction reaction. Fig. 6 shows the impedance spectra of the $Sm_{0.5}Sr_{0.5}CoO_{3-\delta}/Sm_{0.2}Ce_{0.8}O_{1.9}$ (6:4) composite cathode as it changes with respect to $p(O_2)$ and operating temperature. The overall distribution of the impedance spectra and characteristic frequency are very similar to those of the single-phase $Sm_{0.5}Sr_{0.5}CoO_{3-\delta}$ cathode. The electrode resistance of the composite cathode, however, lower than that of pure $Sm_{0.5}Sr_{0.5}CoO_{3-\delta}$. In particular, attempts to improve the electrode resistance of $Sm_{0.5}Sr_{0.5}CoO_{3-\delta}/Sm_{0.2}Ce_{0.8}O_{1.9}$ (6:4) are highly effective at a relatively low temperature range of 400–600 °C.

3.3. Model for cathode reactions

A three-semicircle model with constant phase elements (CPEs) for the impedance is utilized to analyze the oxygen reduction reaction on the single-phase $Sm_{0.5}Sr_{0.5}CoO_{3-\delta}$ and composite $Sm_{0.5}Sr_{0.5}CoO_{3-\delta}/Sm_{0.2}Ce_{0.8}O_{1.9}$ (6:4) cathodes. The resistance values of the electrolyte and electrode are represented as R_e and R_c, respectively. The resistance values of the electrode are broken down into the elements $R_{c,HF}$, $R_{c,MF}$ and $R_{c,LF}$, which represent the resistance in the high, medium, and low frequency regions, respectively. Fig. 7 shows the equivalent circuit, and the individual semicircles defined in the complex plane are shown in Fig. 8. Generally, cathode reactions related to the oxygen reduction mechanism include the following:

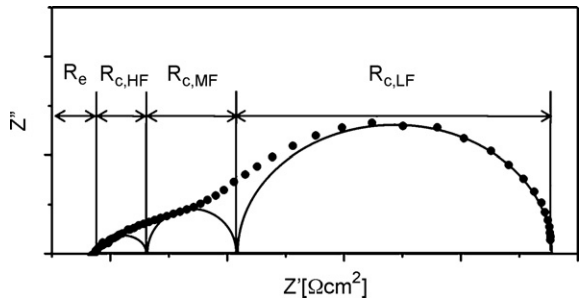

Fig. 8. Electrolyte and electrode resistances defined in the complex plane. $^*R_e$: electrolyte resistance; $R_{c,HF}$: electrode resistance at high frequency; $R_{c,LF}$: electrode resistance at medium frequency; $R_{c,LF}$: electrode resistance at low frequency.

Table 1
Activation energy (E_a) of $Sm_{0.5}Sr_{0.5}CoO_{3-\delta}$ with respect to oxygen partial pressure and frequency range.

$p(O_2)$ (atm)	E_a (eV)			
	High freq.	Medium freq.	Low freq.	Overall freq.
0.0002	1.35	0.80	0.02	0.06
0.002	1.35	0.72	0.08	0.20
0.02	1.21	0.88	0.10	0.64
0.2	1.21	0.96	0.20	0.82
1	1.21	1.01	0.36	0.93

Table 2
Activation energy (E_a) of $Sm_{0.5}Sr_{0.5}CoO_{3-\delta}/Sm_{0.2}Ce_{0.8}O_{1.9}$ with respect to oxygen partial pressure and frequency range.

$p(O_2)$ (atm)	E_a (eV)			
	High freq.	Medium freq.	Low freq.	Overall freq.
0.0002	0.99	0.55	0.02	0.04
0.002	0.96	0.60	0.03	0.08
0.02	0.94	0.49	0.04	0.30
0.2	0.98	0.53	0.22	0.54
1	1.00	0.59	0.21	0.59

(i) gas phase diffusion of the oxygen molecule,
(ii) adsorption of a gas phase oxygen molecule to the cathode surface,
(iii) dissociation of an adsorbed oxygen molecule to the oxygen atom,
(iv) ionization of the adsorbed oxygen molecule,
(v) Surface diffusion of the adsorbed oxygen,
(vi) Ionic conduction of the adsorbed oxygen ion in the bulk electrode,
(vii) Ionic transfer at the interface between the electrode and the electrolyte.

The cathode reaction on the MIEC occurs not only at the triple phase boundary (TPB), but also at the two-phase boundary, as at the cathode surface. Thus, the reactions in steps (i) and (ii) occur throughout the cathode surface and the bulk cathode. Moreover, they are linked to each other. In current research, it has been found that steps (i), (vi) and (vii) are involved as RDSs in the overall oxygen reduction reaction of the cathode. These reaction steps have different time constants; hence, each reaction is characterized in a different frequency range of impedance spectroscopy. Additionally, the reaction steps are linked in a complex manner, due to the properties of the MIEC. The proposed model is based on the following assumptions: (1) the reactions are locally reversible, (2) chemical reactions are based on Langmuir-type

Table 3
Elementary steps and corresponding reaction orders (n) related to cathode reaction.

Elementary steps	Reaction order (n)
Set 1	
$O_2(gas) \rightarrow O_{2,ad}$	1
$O_{2,ad} \rightarrow 2O_{ad}$	1
$O_{ad} + e^- \rightarrow O_{ad}^-$	3/8
$O_{ad}^- + e^- \rightarrow O_{ad}^{2-}$	1/8
$O_{ad}^{2-} + V_O^{\bullet\bullet} \rightarrow O_O^x$	0
Set 2	
$O_2\ (gas) + 2e^- \rightarrow 2O_{ad}^-$	2/3
$O_{ad}^- + e^- \rightarrow O_{ad}^{2-}$	1/8
$O_{ad}^{2-} + V_O^{\bullet\bullet} \rightarrow O_O^x$	0
Set 3	
$O_2(gas) \rightarrow O_{2,ad}$	1
$O_{2,ad} \rightarrow 2O_{ad}$	1
$O_{ad} + 2e^- + V_O^{\bullet\bullet} \rightarrow O_O^x$	1/4

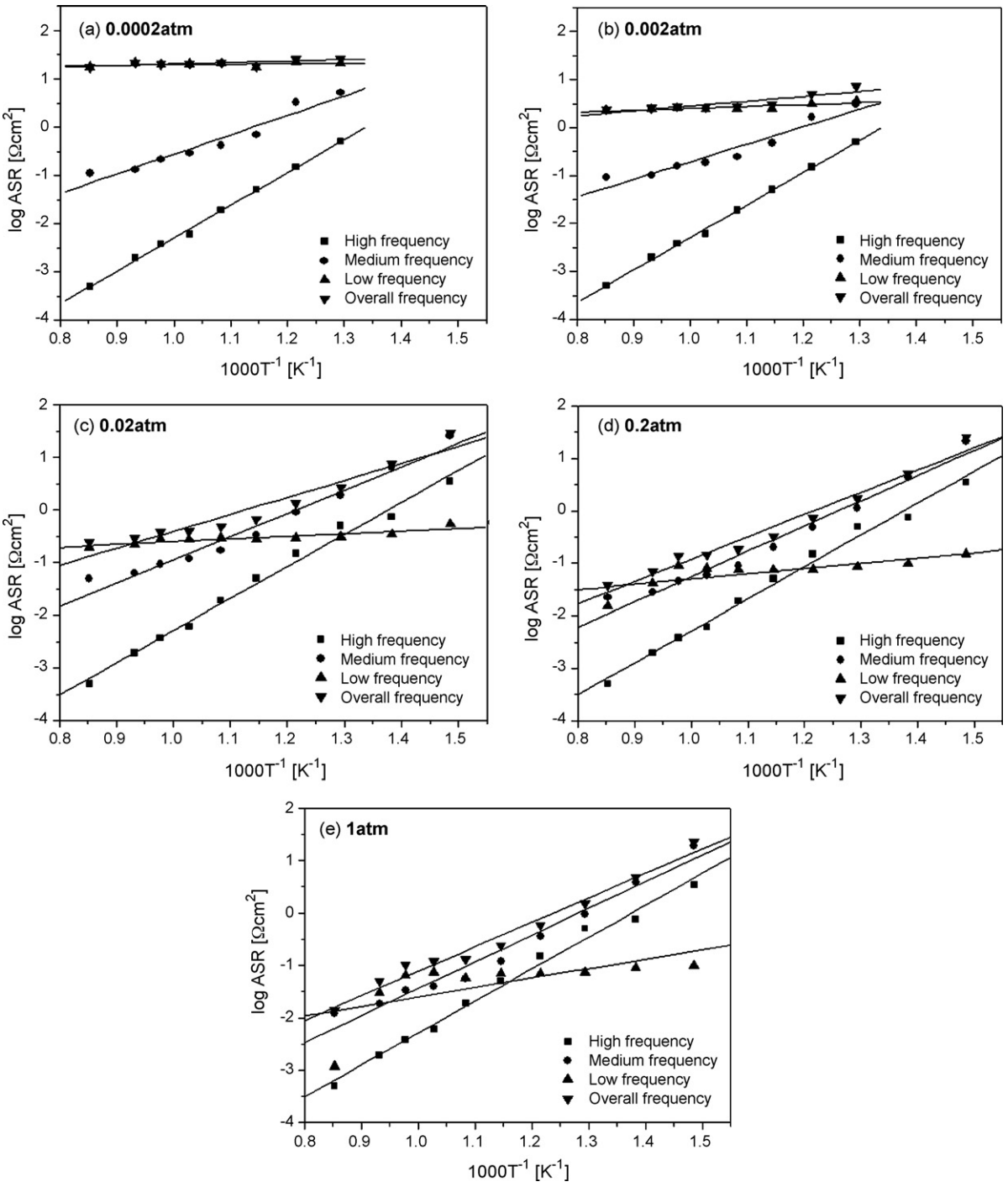

Fig. 9. Variation in electrode resistance of $Sm_{0.5}Sr_{0.5}CoO_{3-\delta}$ as a function of oxygen partial pressure and frequency range.

kinetics, and (3) electrochemical reactions obey the Butler–Volmer equation.

3.4. Area specific resistance and E_a with frequency

The electrode resistance values, for each impedance frequency range, of $Sm_{0.5}Sr_{0.5}CoO_{3-\delta}$ and $Sm_{0.5}Sr_{0.5}CoO_{3-\delta}/Sm_{0.2}Ce_{0.8}O_{1.9}$ (6:4), as a function of temperature and $p(O_2)$ are shown in Figs. 9 and 10, respectively. The electrode resistance is represented as the area specific resistance (ASR), and is calculated as follows:

$$\text{ASR } (\Omega\,\text{cm}^2) = R_c \times A$$

$$R_c = \frac{R_{\text{cathode}}}{2(\text{symmetry})}$$

R_{cathode} and A denote the resistance of the cathode minus the ohmic loss and the effective area of the electrode, respectively. R_c represents the electrode resistance taking into account the symmetry effect of the cathode. R_{cathode} is calculated from the distance between the high-frequency and low-frequency intercepts of the semicircle at the real axis (Z'-axis). Single-phase $Sm_{0.5}Sr_{0.5}CoO_{3-\delta}$ and its composite show similar behaviour throughout the overall temperature and $p(O_2)$ ranges. It is possible that considerable improvement in the cathode performance

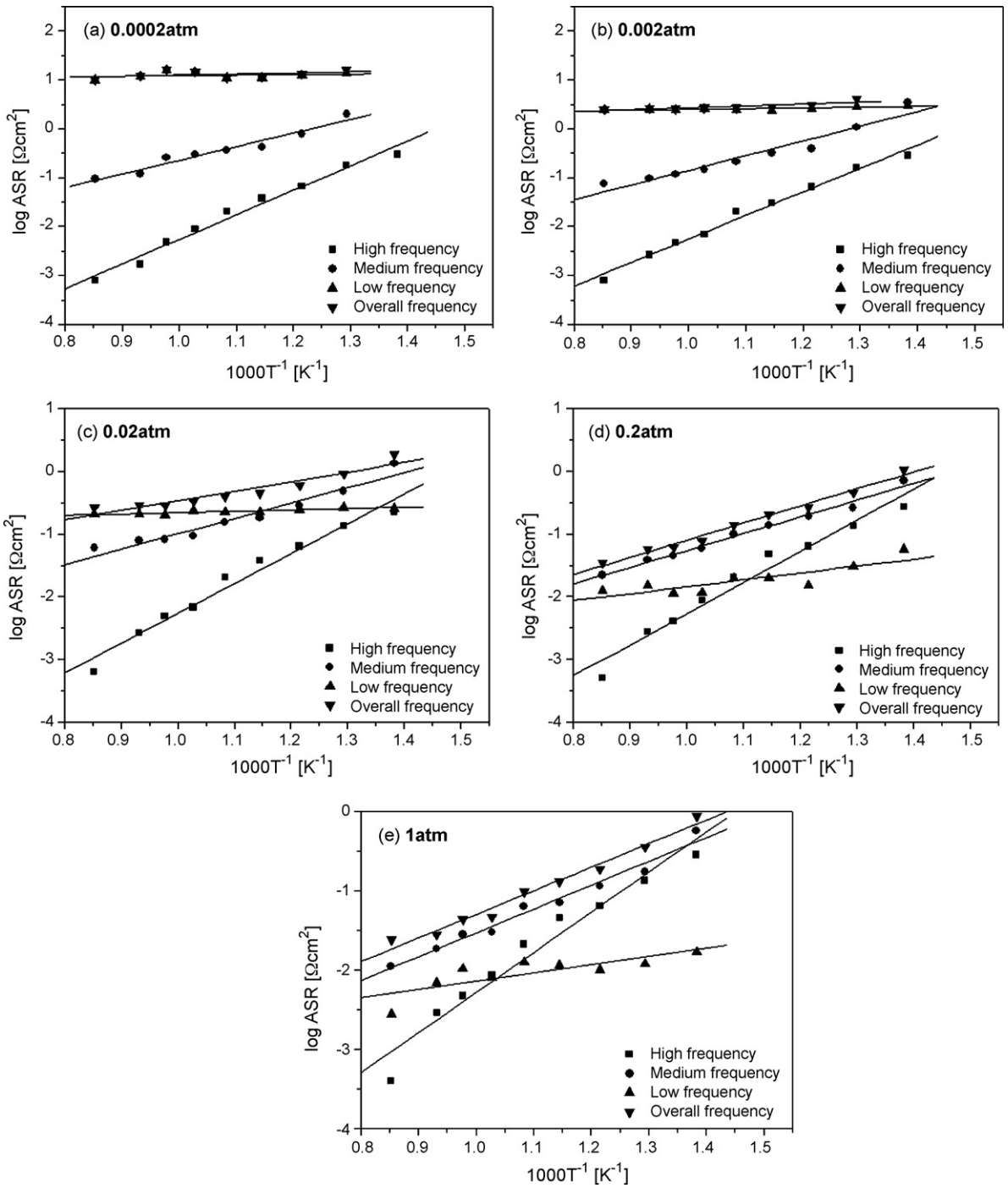

Fig. 10. Variations in electrode resistance of $Sm_{0.5}Sr_{0.5}CoO_{3-\delta}/Sm_{0.2}Ce_{0.8}O_{1.9}$ (6:4) as a function of oxygen partial pressure and frequency range.

occurs because $Sm_{0.5}Sr_{0.5}CoO_{3-\delta}$ is an excellent ionic and electronic conductor and because the reduction reaction takes place at the two-phase boundary of the cathode surface as well as at the TPB. Thus, the oxygen reduction mechanism is also similar in each case.

The activation energy (E_a) is shown in Tables 1 and 2 as a function of frequency and $p(O_2)$ value. The activation energy of the resistance at low frequency shows low values from 0.02 to 0.36 eV in the $p(O_2)$ range of 0.0002–1 atm for $Sm_{0.5}Sr_{0.5}CoO_{3-\delta}$. The electrode resistance at low frequency is independent of temperature at a constant $p(O_2)$, with the exception of a deviation at the high-temperature range with a relatively high $p(O_2)$ range (0.2–1 atm). Thus, the electrode resistance at low frequency corresponds to the behaviour of the gas phase diffusion of oxygen molecules. The high E_a value for $R_{c,HF}$ is independent of temperature. This indicates that the impedance response at high frequency is governed by charge transfer, such as oxygen ion transfer, at the interface between the electrode and the electrolyte. These results are also supported by the ALS (Adler–Lane–Steele) model as well as by several other research results [5,14,16]. The activation energy at high and medium frequencies for the composite cathode decreases compared with the pure $Sm_{0.5}Sr_{0.5}CoO_{3-\delta}$ cathode due to enhancement of reaction activity for each frequency range. This results in the enhancement of both interface adhesion to the electrolyte and particle connection, and improvement in ionic conduction. It is certain that $R_{c,MF}$

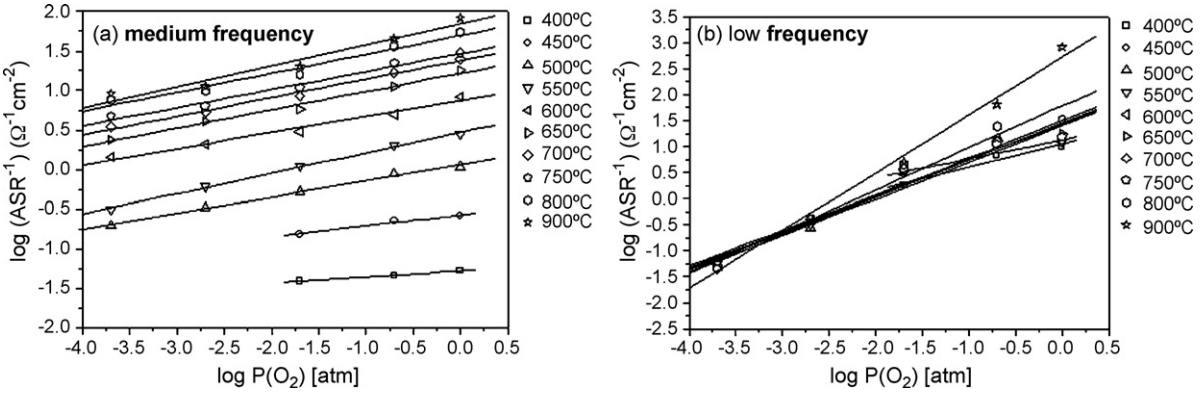

Fig. 11. Plots of ASR^{-1} vs. $p(O_2)$ at various temperatures for $Sm_{0.5}Sr_{0.5}CoO_{3-\delta}$: (a) medium frequency ($R_{c,MF}$) and (b) low frequency ($R_{c,LF}$).

largely affects the overall reaction within a defined temperature and $p(O_2)$ range.

Electrode resistance is governed by $R_{c,LF}$ at all temperature ranges for low $p(O_2)$ values of 0.0002 and 0.002 atm. The electrode resistance is governed by $R_{c,MF}$ at a low temperature range of 400–600 °C at 0.02–1 atm. However, R_c is largely affected by $R_{c,LF}$ at an intermediate temperature range of 700–800 °C. These results are reasonable because the oxygen diffusivity of MIEC is sufficiently high (typically $D_k > 10^{-7}$ to 10^{-8} cm^2 s^{-1} above 800 °C for 0.7–1 atm) at high temperatures and high $p(O_2)$ values [10,16].

3.5. $p(O_2)$ dependence of cathode reaction

The reaction paths of the MIEC cathode material have highly complex links, and the reaction takes place throughout the surface of the two-phase boundary and TPB, due to its high ionic conductivity as compared with a conventional cathode such as LSM. Thus, the establishment of the exact reaction formula is difficult. However, the main RDSs of the MIEC can be determined through an expansion of the basic reaction steps. Reactions with different time constants influence each other to the point that a fluctuation in the reaction order occurs. The overall cathode reaction is considered as follows:

$$O_2(gas) + 4e^- + 2V_O^{\bullet\bullet} \rightarrow 2O_O^x$$

where $V_O^{\bullet\bullet}$ and O_O^x denote an oxygen vacancy and an oxygen ion in the lattice sites, respectively. This overall reaction can be divided into several elementary steps. Table 3 shows the relationship between the elementary steps and the reaction order.

The $R_{c,HF}$ values for $Sm_{0.5}Sr_{0.5}CoO_{3-\delta}$ and $Sm_{0.5}Sr_{0.5}CoO_{3-\delta}/Sm_{0.2}Ce_{0.8}O_{1.9}$ (6:4) are constant, as shown in Figs. 9 and 10. The $R_{c,MF}$ and $R_{c,LF}$ for $Sm_{0.5}Sr_{0.5}CoO_{3-\delta}$ and $Sm_{0.5}Sr_{0.5}CoO_{3-\delta}/Sm_{0.2}Ce_{0.8}O_{1.9}$ (6:4) show similar behaviour; but, it appears that effects other than gas phase diffusion are involved in the cathode reaction in the low-frequency region of $Sm_{0.5}Sr_{0.5}CoO_{3-\delta}$. Figs. 11 and 12 present electrode resistance and $p(O_2)$ values for the medium- and low-frequency regions. A constant slope of 1/4 in the medium-frequency region for both $Sm_{0.5}Sr_{0.5}CoO_{3-\delta}$ and $Sm_{0.5}Sr_{0.5}CoO_{3-\delta}/Sm_{0.2}Ce_{0.8}O_{1.9}$ (6:4) is evident, and this indicates that a similar reaction mechanism is involved throughout the temperature range. The behaviour of $R_{c,LF}$ in $Sm_{0.5}Sr_{0.5}CoO_{3-\delta}$ at low temperatures is somewhat different compared with that at high temperatures. This implies that some factors have an effect on the reaction mechanism at low temperatures. Figs. 11(a) and 12(a) and Table 4 show a 1/4 power $p(O_2)$ dependence in the medium-frequency range for $Sm_{0.5}Sr_{0.5}CoO_{3-\delta}$ and $Sm_{0.5}Sr_{0.5}CoO_{3-\delta}/Sm_{0.2}Ce_{0.8}O_{1.9}$ (6:4); This feature indicates that the ionic conduction of oxygen in the bulk cathode is the RDS. The relationship between R_c and $p(O_2)$ is given by

$$\frac{1}{R_c} \propto p(O_2)^n$$

The most viable improvement in electrode resistance occurs with addition of the $Sm_{0.2}Ce_{0.8}O_{1.9}$ electrolyte material and contributes to $R_{c,MF}$, as shown in Table 5. The enhancement in $R_{c,HF}$ and $R_{c,LF}$ is insignificant. Electrode resistance at medium frequency is also greatly improved at relatively low temperatures below 600 °C. This shows that oxygen diffusion at the bulk cathode is a limiting factor in $Sm_{0.5}Sr_{0.5}CoO_{3-\delta}$ operation at medium-frequency as the temperature decreases. These results are very consistent with the results of Esquirol et al. [9]. In particular, the MIEC composite cathode does not improve the surface kinetics, as in the surface exchange coefficient (k). The surface oxygen exchange rate is determined by an isotopic oxygen exchange, as measured by secondary ion mass

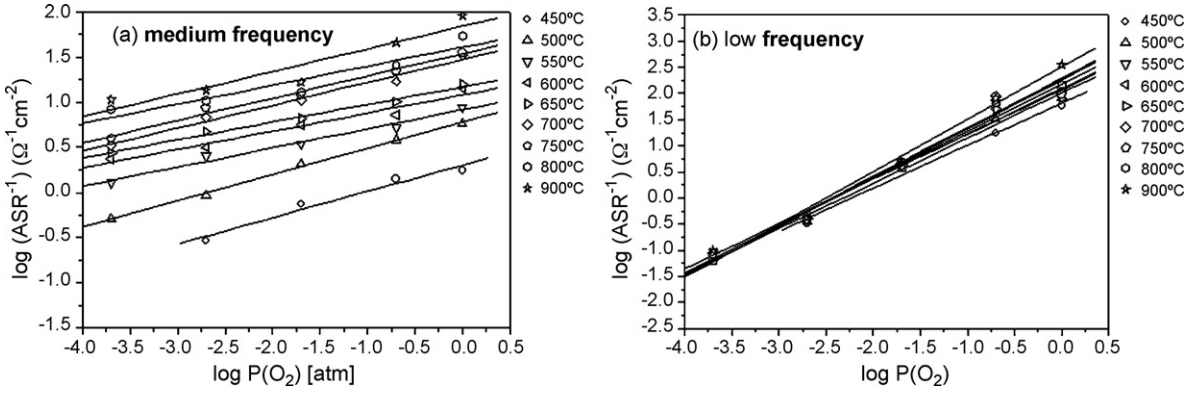

Fig. 12. Plots of ASR^{-1} vs. $p(O_2)$ at various temperatures for $Sm_{0.5}Sr_{0.5}CoO_{3-\delta}/Sm_{0.2}Ce_{0.8}O_{1.9}$ (6:4): (a) medium frequency ($R_{c,MF}$) and (b) low frequency ($R_{c,LF}$).

Table 4
Reaction orders for $Sm_{0.5}Sr_{0.5}CoO_{3-\delta}/Sm_{0.2}Ce_{0.8}O_{1.9}$ and $Sm_{0.5}Sr_{0.5}CoO_{3-\delta}/Sm_{0.2}Ce_{0.8}O_{1.9}$ at various frequency ranges and temperatures.

Temperature (°C)	Reaction order (n)			
	$Sm_{0.5}Sr_{0.5}CoO_{3-\delta}$		$Sm_{0.5}Sr_{0.5}CoO_{3-\delta}/Sm_{0.2}Ce_{0.8}O_{1.9}$ (6:4)	
	MF	LF	MF	LF
400	–	0.44	–	–
450	–	0.36	–	0.82
500	0.20	0.70	0.29	0.86
550	0.26	0.71	0.21	0.90
600	0.20	0.68	0.20	0.86
650	0.23	0.72	0.20	0.85
700	0.24	0.69	0.25	0.95
750	0.23	0.69	0.25	0.94
800	0.24	0.81	0.21	0.93
900	0.27	1.11	0.25	1.00

MF: medium frequency; LF: low frequency.

Table 5
Electrode resistances ($\Omega\,cm^2$) for $Sm_{0.5}Sr_{0.5}CoO_{3-\delta}$ and $Sm_{0.5}Sr_{0.5}CoO_{3-\delta}/Sm_{0.2}Ce_{0.8}O_{1.9}$ (6:4).

Temperature (°C)	$Sm_{0.5}Sr_{0.5}CoO_{3-\delta}$				$Sm_{0.5}Sr_{0.5}CoO_{3-\delta}/Sm_{0.2}Ce_{0.8}O_{1.9}$ (6:4)			
	$R_{c,HF}$	$R_{c,MF}$	$R_{c,LF}$	R_c	$R_{c,HF}$	$R_{c,MF}$	$R_{c,LF}$	R_c
450	1.500	13.10	0.700	15.30	0.561	2.669	0.517	3.747
500	1.000	3.836	0.620	5.456	0.337	0.962	0.537	1.836
550	0.300	1.811	0.590	2.701	0.128	0.577	0.500	1.205
600	0.100	0.671	0.560	1.331	0.095	0.355	0.450	0.900
650	0.038	0.344	0.600	0.982	0.041	0.306	0.450	0.797
700	0.012	0.237	0.550	0.799	0.017	0.189	0.475	0.682
750	0.008	0.186	0.564	0.758	0.010	0.164	0.410	0.583
800	0.004	0.127	0.450	0.581	0.005	0.157	0.418	0.580
900	0.001	0.099	0.400	0.500	0.001	0.120	0.419	0.540

R_c: overall electrode resistance, $R_{c,HF}$: electrode resistance at high frequency, $R_{c,MF}$: electrode resistance at medium frequency, $R_{c,LF}$: electrode resistance at low frequency. $p(O_2) = 0.02$ atm.

spectrometry (SIMS) analysis. In the case of the LSC cathode, the surface can supply sufficient active sites for oxygen reduction, due to its high ionic and electronic conductivity, so that the surface reaction rates are very fast compared with other processes (typically, k: 10^{-5} cm s^{-1} at 800 °C, 1 atm) [10,16]. A reaction order of 1/2 for R_c and $p(O_2)$ generally represents the surface diffusion involved in atomic oxygen [3,11–13]. In the present study, however, a reaction order of 1/2 is not shown by any of the results. These results and data clearly indicate that the ionic conduction of oxygen in the bulk cathode is related to $R_{c,MF}$.

The reaction order (n) for $Sm_{0.5}Sr_{0.5}CoO_{3-\delta}$ at low frequency shows a fluctuation in the range of 0.4–1.1 as the temperature increases. In particular, the reaction step related to $R_{c,LF}$ changes according to the temperature range, as the reaction order approaches 0.4 at 400–500 °C and 1 at temperatures above 800 °C. At approximately $n = 0.4$, an oxygen surface reduction reaction related to the electron along with the gas phase diffusion of oxygen is partially involved in the RDS, based on an analysis of the reaction order. The reaction order of the oxygen reduction reaction related to atomic oxygen and the electron is generally represented as 3/8, 2/3 and 1/8, as shown in Table 3. The reduction reaction step of atomic oxygen participates in the RDS at low frequency, along with the oxygen gas diffusion limitation. For single-phase $Sm_{0.5}Sr_{0.5}CoO_{3-\delta}$, gas phase limitation is dominant at high temperatures due to the enhanced oxygen surface kinetics and bulk conduction, since the reaction order approaches 1 as the temperature increases. For the $Sm_{0.5}Sr_{0.5}CoO_{3-\delta}/Sm_{0.2}Ce_{0.8}O_{1.9}$ (6:4) composite cathode, the reaction order at low frequency throughout the temperature range approaches 1, unlike that of $Sm_{0.5}Sr_{0.5}CoO_{3-\delta}$. Table 5 provides further evidence of the variation in reaction order by using a composite at low frequency. A small enhancement of $R_{c,LF}$ over the entire temperature range is shown by utilizing the composite. This indicates that the oxygen reduction processes, such as charge transfer or ionic conduction, are improved compared with the $Sm_{0.5}Sr_{0.5}CoO_{3-\delta}$ cathode. Electrode resistances at high- and medium-frequency are enhanced by the addition of $Sm_{0.2}Ce_{0.8}O_{1.9}$ at temperatures below 650 °C. This results in an improvement of oxygen ion conduction at the bulk cathode by the addition of electrolyte material at low temperatures.

The resistances of the oxygen reduction reaction related to the electron/atomic oxygen and the ionic conduction of oxygen are partially involved in the oxygen gas phase diffusion limitation at low frequency, due to the complexity of the reaction mechanism in the case of the single-phase MIEC $Sm_{0.5}Sr_{0.5}CoO_{3-\delta}$, although the time constant of each reaction is different. As a result, the $R_{c,LF}$ values of $Sm_{0.5}Sr_{0.5}CoO_{3-\delta}$, the single-phase MIEC, are dominated by the partially mixed reaction of the charge-transfer process and the non-charge transfer process from an intermediate state. The $R_{c,LF}$ values of $Sm_{0.5}Sr_{0.5}CoO_{3-\delta}/Sm_{0.2}Ce_{0.8}O_{1.9}$ (6:4), the composite cathode, are dominated by the non-charge transfer process and diminish the effect of the charge-transfer process.

4. Conclusions

In the present study, the cathodic behaviour of porous-structured single-phase $Sm_{0.5}Sr_{0.5}CoO_{3-\delta}$ and composite $Sm_{0.5}Sr_{0.5}CoO_{3-\delta}/Sm_{0.2}Ce_{0.8}O_{1.9}$ cathodes are studied in terms of $p(O_2)$, the impedance response, E_a and the reaction order at various temperatures. Similar cathode reaction behavior is shown in both $Sm_{0.5}Sr_{0.5}CoO_{3-\delta}$ and $Sm_{0.5}Sr_{0.5}CoO_{3-\delta}/Sm_{0.2}Ce_{0.8}O_{1.9}$. It is concluded that three elementary steps are primarily involved in the cathodic reaction as RDSs. The electrode resistance at high frequency represents the oxygen ion transfer at the interface of the cathode and the electrolyte. The electrode resistance at medium frequency represents the oxygen ion conduction in the

bulk cathode. This is explained from an enhancement of $R_{c,MF}$ for $Sm_{0.5}Sr_{0.5}CoO_{3-\delta}/Sm_{0.2}Ce_{0.8}O_{1.9}$ in a low temperature range as compared with $Sm_{0.5}Sr_{0.5}CoO_{3-\delta}$, the impedance spectra and the reaction order. The electrode resistance at low-frequency for single-phase $Sm_{0.5}Sr_{0.5}CoO_{3-\delta}$ indicates the partially linked reaction steps of a charge transfer process and a non-charge transfer process. The electrode resistance at low frequency for a $Sm_{0.5}Sr_{0.5}CoO_{3-\delta}/Sm_{0.2}Ce_{0.8}O_{1.9}$ composite cathode is explained by a non-charge transfer related to the gas phase diffusion of oxygen. These observations are also verified by the difference in micro-structure and the impedance variation due to the addition of $Sm_{0.2}Ce_{0.8}O_{1.9}$, and thermal cycling and long-term tests. It is expected that the research results will be useful when attempting to understand the cathodic behaviour of a MIEC and that they can assist with the design of a high-performance cathode for a SOFC.

Acknowledgements

This work is an outcome of projects in the development program of Core Technologies for Fuel Cells (CTFC) of the Ministry of Knowledge Economy, and the Brain Korea 21 (BK21) program of the Ministry of Education, Science and Technology of Korea. The authors greatly appreciate the financial support from these organizations.

References

[1] T. Kawada, H. Yokokawa, Key Eng. Mater. 125–126 (1997) 187–248.
[2] M. Gödickemeier, K. Sasaki, L.J. Gauckler, J. Electrochem. Soc. 144 (5) (1997) 1635–1646.
[3] Y. Takeda, R. Kanno, M. Noda, Y. Tomida, O. Yamamoto, J. Electrochem. Soc. 134 (11) (1987) 2656–2661.
[4] A. Barbucci, M. Viviani, M. Panizza, M. Delucchi, G. Cerisola, J. Appl. Electrochem. 35 (2005) 399–403.
[5] J. Deseure, Y. Bultel, L. Dessemond, E. Siebert, P. Ozil, J. Appl. Electrochem. 37 (2007) 129–136.
[6] Q.A. Huang, R. Hui, B. Wang, J. Zhang, Electrochim. Acta 52 (2007) 8144–8164.
[7] C. Xia, W. Rauch, F. Chen, M. Liu, Solid State Ionics 149 (2002) 11–19.
[8] X. Zhang, M. Robertson, S. Yick, C.D. Petit, E. Styles, W. Qu, Y. Xie, R. Hui, J. Roller, O. Kesler, R. Maric, D. Ghosh, J. Power Sources 160 (2006) 1211–1216.
[9] A. Esquirol, J. Kilner, N. Brandon, Solid State Ionics 175 (2004) 63–67.
[10] S. Kim, Y.L. Yang, A.J. Jacobson, B. Abeles, Solid State Ionics 106 (1998) 189–195.
[11] H. Fukunaga, M. Koyama, N. Takahashi, C. Wen, K. Yamada, Solid State Ionics 132 (2000) 279–285.
[12] M. Koyama, C. Wen, T. Masuyama, J. Otomo, H. Fukunaga, K. Yamada, K. Equchi, H. Takahashi, J. Electrochem. Soc. 148 (7) (2001) A795–A801.
[13] T. Horita, K. Yamaji, N. Sakai, H. Yokokawa, A. Weber, E.I. Tiffée, Electrochim. Acta 46 (2001) 1837–1845.
[14] M. Hunsom, L.A. Dunyushkina, S.B. Adler, Korean J. Chem. Eng 23 (5) (2006) 720–725.
[15] E.P. Murray, M.J. Sever, S.A. Barnett, Solid State Ionics 148 (2002) 27–34.
[16] S.B. Adler, J.A. Lane, B.C.H. Steele, J. Electrochem. Soc. 143 (11) (1996) 3554–3564.
[17] J.A. Kilner, R.A.D. Souza, I.C. Fullarton, Solid State Ionics 86–88 (1996) 703–709.
[18] S. Wang, A. Verma, Y.L. Yang, A.J. Jacobson, B. Abeles, Solid State Ionics 140 (2001) 125–133.
[19] L.W. Tai, M.M. Nasrallah, H.U. Anderson, D.M. Sparlin, S.R. Sehlin, Solid State Ionics 75 (1995) 259–271.
[20] L.W. Tai, M.M. Nasrallah, H.U. Anderson, D.M. Sparlin, S.R. Sehlin, Solid State Ionics 76 (1995) 273–283.
[21] F.S. Baumann, J. Fleig, H.U. Habermeier, J. Maier, Solid State Ionics 177 (2006) 1071–1081.
[22] A. Aguadero, M.J. Escudero, M. Pérez, J.A. Alonso, L. Daza, J. Fuel Cell Sci. Tech. 4 (2007) 294–298.
[23] S.W. Baek, C. Lee, J. Bae, Proceedings for FuelCell 2007, The 5th ASME International Conference on Fuel Cell Science, Engineering and Technology Conference, Newyork, USA, 2007.
[24] M. Koyama, C.J. Wen, K. Yamada, J. Electrochem. Soc. 147 (1) (2000) 87–91.
[25] F. Mauvy, J.M. Bassat, E. Boehm, J.P. Manaud, P. Dordor, J.C. Grenier, Solid State Ionics 158 (2003) 17–28.